基于游标效应的高灵敏光纤温度和应变传感器

方莎莎[1]，吴许强[1,2*]，张刚[1]，时金辉[1]，左铖[2]，张伍军[2]，桂磊[2]，俞本立[1,2]

[1]安徽大学信息材料与智能感知安徽省实验室，安徽 合肥 230601；
[2]安徽大学光电信息获取与控制教育部重点实验室，安徽 合肥 230601

摘要 提出一种基于光纤 Sagnac 干涉仪（FSI）和偏振模干涉仪（PMI）级联结构的高灵敏光纤温度和应变传感器。FSI 作为参考干涉仪，是将对温度、应变、弯曲及扭转不敏感的椭圆芯保偏光纤（ECPMF）引入到 Sagnac 环内制得的。PMI 作为传感干涉仪，是对光纤起偏器与末端端面镀金的熊猫型保偏光纤（PMF）的快轴/慢轴以 45°角进行熔接制得的。参考干涉仪的自由光谱区（FSR）易被调整为接近传感干涉仪的 FSR，从而产生光学游标效应，实现灵敏度放大。实验结果表明：所设计的级联传感器的温度灵敏度达 15.56 nm/℃，是单个 PMI 的 11.12 倍；应变灵敏度达 154.04 pm/$\mu\varepsilon$，是单个 PMI 的 11.81 倍。所设计的传感器具有灵敏度高、制作简单、稳定性好等优点，在航空航天、工业生产等领域中具有广阔的应用前景。

关键词 光纤光学；光纤传感器；熊猫型保偏光纤；椭圆芯保偏光纤；游标效应；温度和应变传感器

中图分类号 TN929.11　　　　**文献标志码** A　　　　**doi**：10.3788/CJL202148.0106004

1 引 言

光纤传感器因具有结构简单、体积小、质量轻、抗电磁干扰、灵敏度高等优点，广泛应用于温度[1]、折射率[2]、压力[3]、应变[4]等外界物理量的测量领域。其中光纤温度、应变传感器在过去二十年中得到了广泛的研究，在航天航空、工业生产、安全监测等领域具有广阔的应用前景。常见的光纤温度、应变传感器一般基于光纤光栅或光纤干涉仪结构，其中基于光纤光栅结构[5]的温度、应变传感器的灵敏度通常较低，一般分别在 pm/℃ 和 pm/$\mu\varepsilon$ 量级；而基于法布里-珀罗干涉仪（FPI）[6-7]、马赫-曾德尔干涉仪（MZI）[8-9]及光纤 Sagnac 干涉仪（FSI）[10]等结构的温度、应变传感器，温度灵敏度可以达亚 nm/℃ 甚至 nm/℃ 量级，而应变灵敏度通常在 pm/$\mu\varepsilon$ 量级。

近年来，某些特殊应用领域对光纤温度、应变传感器的灵敏度提出了更高要求，研究人员开始将游标效应作为一种增敏手段应用于光学检测中。目前，基于光学游标效应的干涉仪组合一般有 2 个级联 FPI[11]、2 个级联 MZI[12]、2 个级联 FSI[13-14]或其他混合级联配置[15-16]。控制两个干涉仪的自由光谱区（FSR），使之相近但不相等，从而产生游标效应，实现传感灵敏度的大幅度提升。2019 年，Wang 等[17]将一段空芯光纤熔接到两段多模光纤之间形成单个 MZI，再对 2 个相同的 MZI 进行并联形成级联 MZI 结构的温度传感器，该传感器的灵敏度为 528.5 pm/℃。2019 年，Yang 等[18]将一段硅管拼接到两段单模光纤（SMF）之间形成双级联 FPI 温度传感器，该传感器灵敏度为 183.99 pm/℃。2019 年，Su 等[19]将悬浮芯光纤分别连接到 2×2 3 dB 光纤耦合器输出端，形成级联 FPI 结构的温度传感器，该传感器灵敏度为 153.8 pm/℃。2019 年，Liu 等[20]分别利用熊猫型保偏光纤（PMF）和少模光纤（FMF）形成 FSI 与光纤模态干涉（FMI）级联的应变传感器，该传感器应变灵敏度为 65.71 pm/$\mu\varepsilon$。2019 年，Liu 等[21]将两段 PMF 以 45°角熔接并引入到 Sagnac 环中，形成可以产生游标效应的温度、应变传感器，其温度和应变灵敏度分别为 1.05 nm/℃ 和 58.0 pm/$\mu\varepsilon$。上述级联结构均为级联同一作用机制制造的干涉仪，它们对外界物理量变化响应几乎相同，这将导致级联传感器灵敏度降低。为了增大级联传感器对被测物理量响应的差异，通常需要对参考干涉仪采取隔离措施，这意味着测量的复杂

性和难度将会增加。

　　因此，本文提出一种将椭圆芯保偏光纤（ECPMF）引入到 Sagnac 环内作为参考干涉仪的光纤温度、应变传感器。其中，由于 ECPMF 对温度、应变、弯曲及扭转不敏感，FSI 光谱稳定易控，能为传感干涉仪提供一个基于光学游标效应的"定标主尺"。参考干涉仪级联具有偏振模干涉仪（PMI）结构的传感干涉仪，可实现温度和应变的高灵敏、高准确度传感。

2　传感器结构及传感原理

　　基于 PMI 和 FSI 混合级联结构的所提传感器结构示意图如图 1 所示。在 PMI 中，对末端镀金的一段 PMF 与光纤起偏器输出端 PMF 的快轴/慢轴进行 45°角熔接，光纤起偏器既作为入射光的起偏器又作为反射光的检偏器，由于双折射，正交偏振模在 PMF 中传播时会产生相位差。在温度和应变作用下，双折射的折射率差和光纤长度发生变化，从而导致相位发生变化，进而引起干涉光谱移动。对于 FSI，它是由一个 3 dB 光纤耦合器和一段 ECPMF 制作的 Sagnac 干涉仪。FSI 易受环境扰动甚至受小气流的影响，但本文中 FSI 环内的 ECPMF 对温度、应变、弯曲及扭转不敏感，这里将 3 dB 光纤耦合器输入和输出端 SMF 熔接长度控制得足够短，因此外界扰动对 FSI 的影响可以忽略，制备的 FSI 更适合作为参考干涉仪。通过环形器对这两个干涉仪进行连接，会在输出端得到 FSR 略有差异的干涉谱的叠加，从而形成游标效应。
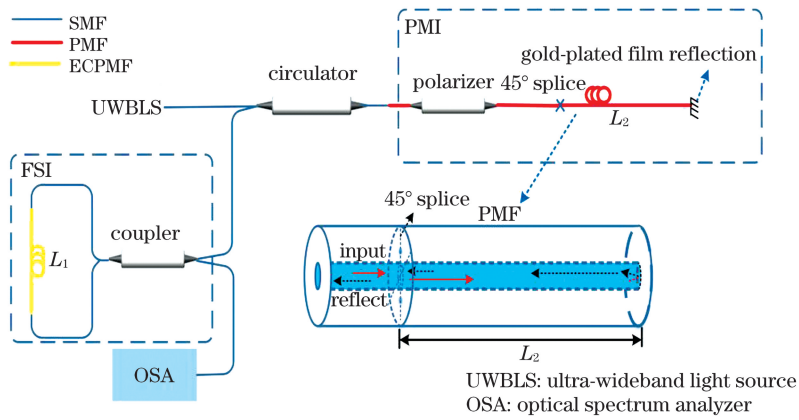

图 1　PMI 与 FSI 混合级联结构的原理图

Fig. 1　Schematic of hybrid cascaded configuration with PMI and FSI

　　FSI 透射谱函数[13]可以表示为

$$T_{\mathrm{FSI}}(\lambda) = \sin^2\left(\frac{\pi B_{\mathrm{a}} L_1}{\lambda}\right), \tag{1}$$

式中：B_{a} 为 ECPMF 双折射参数；L_1 为 ECPMF 的长度；λ 为光源的波长。由（1）式可知，FSI 的输出功率随波长变化，FSI 的 FSR 可以推导为

$$F_{\mathrm{FSI}} = \frac{\lambda^2}{B_{\mathrm{a}} L_1}. \tag{2}$$

　　忽略 PMI 的损耗，假设 PMI 的输入光强为 I_0，则输出光强[22]可表示为

$$I = \frac{I_0}{2}(1 - \cos\varphi), \tag{3}$$

$$\varphi = \frac{2\pi}{\lambda} B_{\mathrm{b}} 2L_2, \tag{4}$$

式中：φ 为 PMF 两束光的相位差；L_2 为 PMF 长度；B_{b} 为 PMF 双折射参数。由于谐振波长光谱需满足条件 $\varphi = 2m\pi$（m 为整数），共振波长可以描述为

$$\lambda = \frac{2B_{\mathrm{b}} L_2}{m}. \tag{5}$$

　　根据（5）式，可以推导出 PMI 的 FSR，表达式为

$$F_{\mathrm{PMI}} = \frac{\lambda^2}{2B_{\mathrm{b}} L_2}. \tag{6}$$

　　在混合级联结构中，级联传感器的输出谱等于各自输出谱的乘积，因此最终输出谱是由一系列振幅不同的条纹组成的周期性包络，包络函数的 FSR[23]可以表示为

$$F_{\mathrm{envelope}} = \frac{F_{\mathrm{PMI}} \times F_{\mathrm{FSI}}}{|F_{\mathrm{PMI}} - F_{\mathrm{FSI}}|}. \tag{7}$$

　　当温度和应变改变时，传感干涉仪的 PMI 波长会发生飘移。然后将干涉谱包络的波长飘移放大一定的倍数，放大系数 M[14]可以表示为

$$M = \frac{F_{\mathrm{FSI}}}{|F_{\mathrm{PMI}} - F_{\mathrm{FSI}}|}. \tag{8}$$

　　由（8）式可知，当 F_{PMI} 和 F_{FSI} 接近但不相等

时,可以提高 PMI 的温度和应变灵敏度。干涉谱包络的温度和应变灵敏度 S_1、S_2 可以分别表示为

$$S_1 = \frac{\mathrm{d}\lambda_{\mathrm{envolope}}}{\mathrm{d}T} = 2M \times \lambda \left(\frac{1}{B_b} \frac{\partial B_b}{\partial T} + \frac{1}{L_2} \frac{\partial L_2}{\partial T} \right),$$

(9)

$$S_2 = \frac{\mathrm{d}\lambda_{\mathrm{envolope}}}{\mathrm{d}\varepsilon} = 2M \times \lambda \left(\frac{1}{B_b} \frac{\partial B_b}{\partial \varepsilon} + \frac{1}{L_2} \frac{\partial L_2}{\partial \varepsilon} \right),$$

(10)

式中:$\frac{1}{B_b} \frac{\partial B_b}{\partial T}$ 和 $\frac{1}{B_b} \frac{\partial B_b}{\partial \varepsilon}$ 分别为温度和应变对双折射参数的影响;$\frac{1}{L_2} \frac{\partial L_2}{\partial T}$ 和 $\frac{1}{L_2} \frac{\partial L_2}{\partial \varepsilon}$ 分别为温度和应变对 PMF 长度的影响。从(9)、(10)式可以看出,干涉谱包络的温度和应变灵敏度与光纤长度、PMF 双折射参数有关。

3　传感器制作和性能仿真

3.1　传感器制作

在 PMI 和 FSI 混合级联传感器中,PMI 是通过 CO_2 激光熔接机(Fujikura LZM-100)对一段末端镀金的 PMF(YOFC PM1017-A)和光纤起偏器输出端 PMF 的快轴/慢轴进行 45°熔接制成的。选择熔接机的熔接模式为 PANDA 125,放电功率和放电时间分别设置为 20 bit 和 1500 ms,左侧光纤 θ 角度调整为 45°,熔接图像如图 2(a)所示,其中 PMF 的纤芯和包层直径分别为 6.5 μm 和 125 μm,实验中所使用 PMF 的长度为 0.94 m。级联的 FSI 是将一段 ECPMF(IVG PME-1300-125)熔接到一个单模 2×2 3 dB 耦合器中制成的。选择熔接机的熔接模式为 SM 125,放电功率和放电时间分别设置为 20 bit 和 2000 ms。熔接图像和 ECPMF 光纤截面如图 2(b)所示,其中 SMF 纤芯和包层直径分别为 8 μm 和 125 μm,ECPMF 长轴半径、短轴半径和包层直径分别为 3 μm、1 μm、125 μm,ECPMF 的拍长小于 30 mm,实验中所使用 ECPMF 的长度为 10 m。PMI 和 FSI 通过光纤环形器(circulator)连接,形成级联传感器。
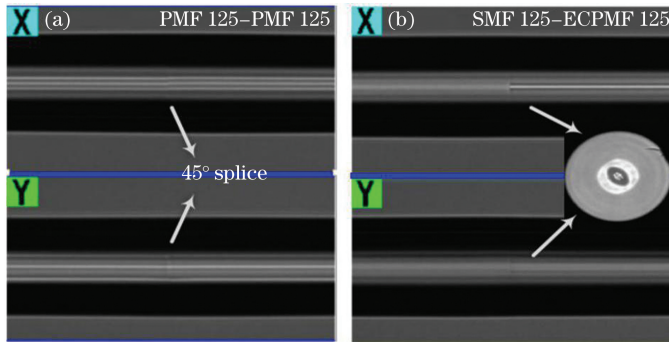

图 2　光纤熔接图像。(a)熊猫 PMF 与熊猫 PMF 45°熔接;(b) SMF 与 ECPMF 熔接

Fig. 2　Fusion images of fiber optic. (a) Splice of panda PMFs at an angle of 45°; (b) splice of SMF and ECPMF

3.2　传感器性能仿真

为了更加直观地说明游标效应可以提高传感器的灵敏度,分别对单个 FSI、单个 PMI 及级联传感器的输出光谱进行仿真。仿真参数分别设为 $L_1 = 10$ m,$L_2 = 0.94$ m,$B_a = 0.6 \times 10^{-4}$,$B_b = 3.5 \times 10^{-4}$,$I_0 = 0.003$ mW,由(8)式计算得理论放大因子 M 为 11.34,仿真结果如图 3 所示。FSI 的 FSR 为 3.15 nm,PMI 的 FSR 为 2.87 nm。当外界物理量变化引起 PMF 的双折射参数 B_b 从 3.5×10^{-4} 增加至 3.51×10^{-4} 时,单个 PMI 的干涉光谱红移 1.12 nm,级联传感器的干涉光谱红移 12.7 nm,放大倍数为 11.34,这与理论计算结果一致。

4　实验装置与结果

4.1　温度传感特性实验研究

温度测量实验装置如图 4 所示,超宽带光源(UWBLS)作为输入光源,该级联传感器的透射光谱由分辨率为 0.02 的光谱分析仪(OSA,Yokogawa AQ6370C)接收,传感探头被放置在精度为 0.01 ℃的加热板上。在光纤自然放置的状态下,先使信号光分别经过单个 FSI 和单个 PMI,得到的干涉光谱如图 5(a)所示;然后使信号光经过级联传感器,得到的干涉光谱如图 5(b)所示。由图 5 可知,PMI 和 FSI 的 FSR 分别为 2.83 nm 和 3.1 nm,级联传感器的 FSR 为 35 nm,根据(2)式计算得到 ECPMF 的
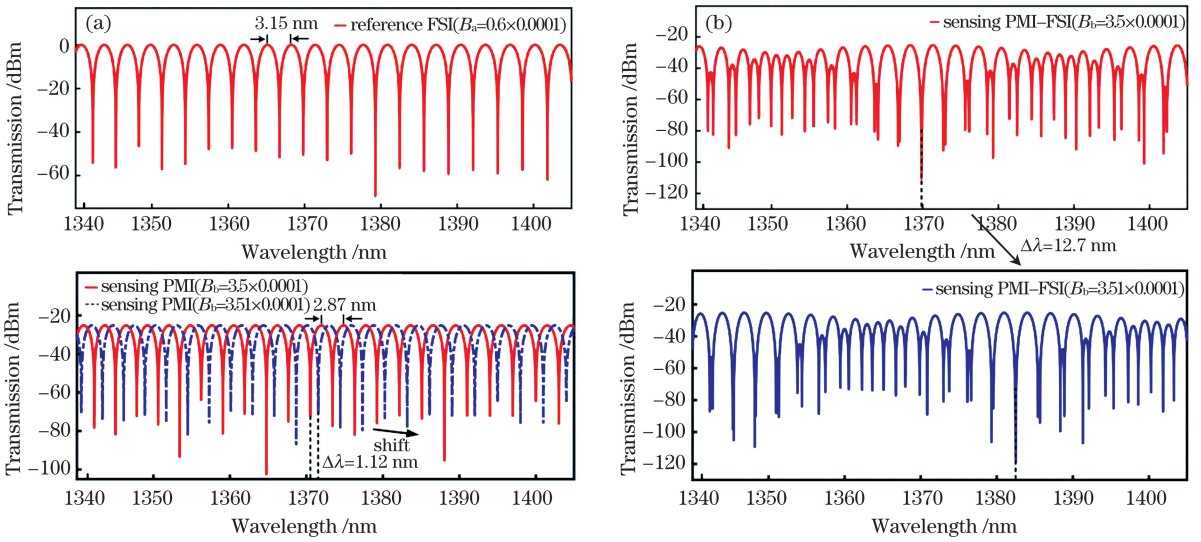
图 3　传感器仿真输出光谱。(a) FSI 和 PMI 光谱及其移动；(b)级联传感器光谱及其移动

Fig. 3　Simulated output spectra of sensors. (a) FSI spectrum , PMI spectrum and its movement；(b) spectra and its movement of cascaded sensor
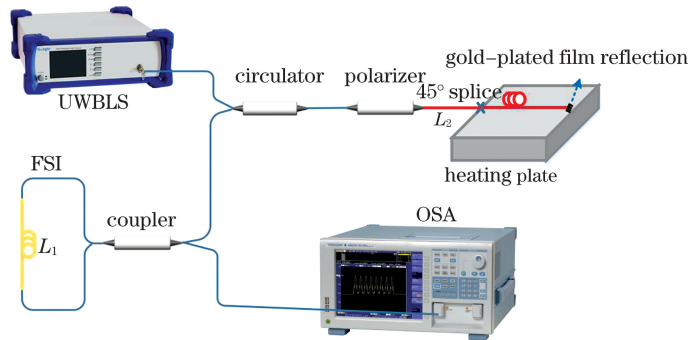

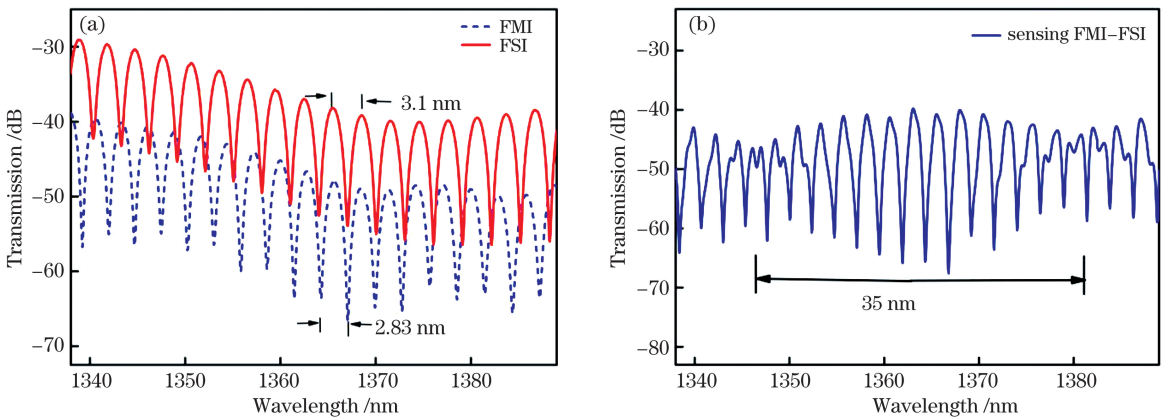图 4　温度传感实验装置

Fig. 4　Experimental setup of temperature sensing

图 5　实测干涉光谱。(a)单个 FSI 和 PMI；(b)级联传感器

Fig. 5　Measured interference spectra. (a) Single FSI and PMI；(b) cascaded sensor

B_a 值为 $6×10^{-5}$，在 1550 nm 下实际测得的拍长为 25.8 mm，与产品参数一致。PMI 与 FSI 通过环形器级联后产生游标效应，由（8）式计算可得游标效应的放大倍数为 11.48，与仿真结果基本吻合，误差主

要来自于读取光谱时的读数误差。

为了研究 PMI 的温度传感特性，分别对单个 PMI 和级联传感器的温度灵敏度进行测试。将 PMI 固定于加热板上，在实验中，温度测量范围为

30～37 ℃,步长为 1 ℃,每个温度状态保持 20 min。单个 PMI 和级联传感器干涉光谱如图 6 所示,随着温度的升高,干涉光谱均发生蓝移,级联传感器的包络波长漂移量远高于单个 PMI 波长漂移量,温度灵敏度得到了显著提高。单个 PMI 与级联传感器的温度灵敏度如图 7 所示,测得单个 PMI 的温度灵敏度分别为 1.40 nm/℃ 和 1.38 nm/℃,级联传感器的温度灵敏度为 15.56 nm/℃,约是单个 PMI 的 11.12,与理论值 11.34 基本一致。

为了验证 FSI 的温度相对不敏感性,将 FSI 固定于加热板上,测得单个 FSI 干涉光谱的温度响应,结果如图 8(a)所示,随着温度的升高,干涉光谱发生蓝移。单个 FSI 的温度灵敏度如图 8(b)所示,测得单个 FSI 的温度灵敏度分别为 168.38 pm/℃ 和 157.44 pm/℃,
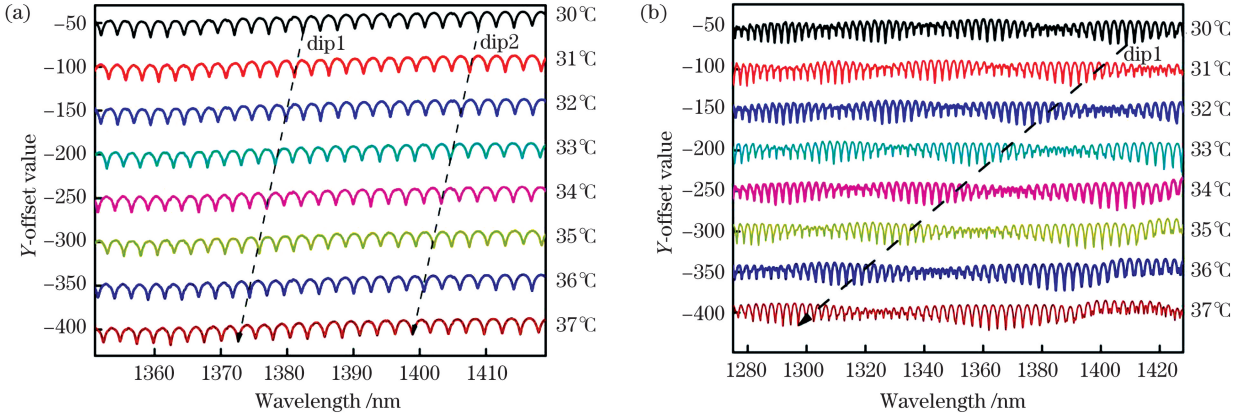

图 6　传感器在不同温度下的干涉光谱。(a)单个 PMI;(b)级联传感器

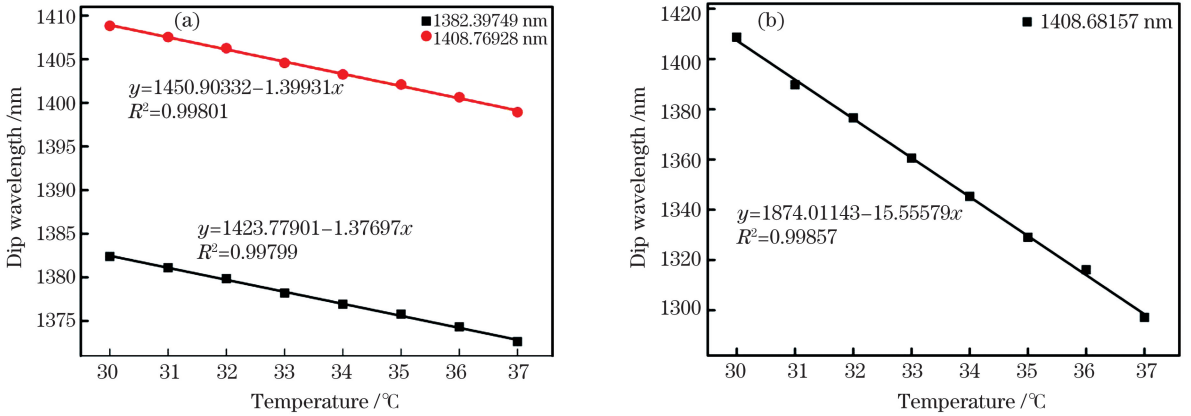Fig. 6　Interference spectra of the sensor under different temperatures. (a) Single PMI; (b) cascaded sensor

图 7　波长漂移与温度的关系。(a)单个 PMI;(b)级联传感器

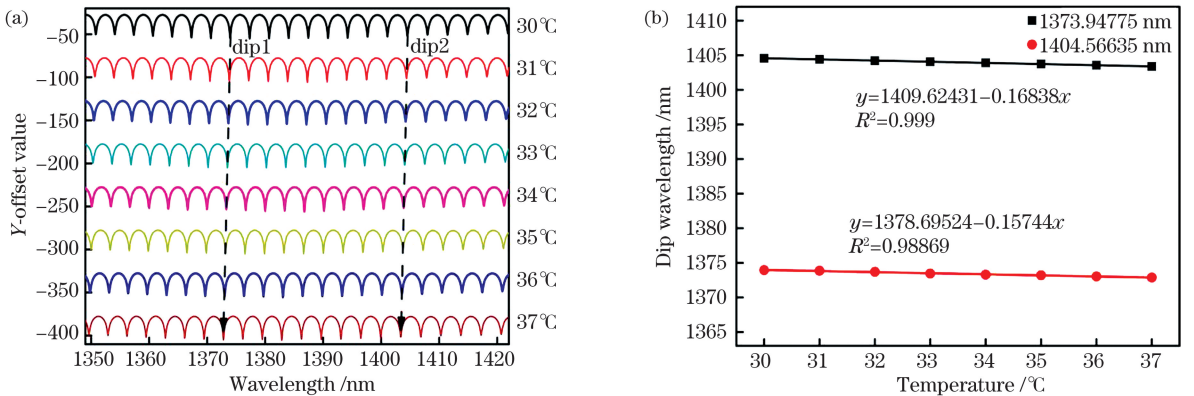Fig. 7　Relationship between wavelength shift and temperature. (a) Single PMI; (b) cascaded sensor

图 8　FSI 温度响应。(a)光谱漂移;(b)波长漂移与温度的关系

Fig. 8　Temperature response of FSI. (a) Spectra shift; (b) relationship between wavelength shift and temperature

约是 PMI 温度灵敏度的 1/8。因此相对于 PMI，FSI 干涉光谱具有温度不敏感性，用 ECPMF 制备的 FSI 更适合作为参考干涉仪。

4.2　应变传感特性实验研究

为了研究 PMI 的应变传感特性，通过光学黏合剂（NORLAND 81）将 PMI 固定于精度为 1 μm 的微位移平台（Thorlabs，KMTS25E/M）上，平台间的距离为 40 cm，通过软件控制其中一个微位移平台向外移动，每次位移为 16 μm，PMI 产生的应变量为 40 με。分别用光谱分析仪记录每次应变下对应的干涉光谱，在实验中应变测量范围为 0～280 με，电位移平台示意图如图 9 所示。接下来分别对单个 PMI 和级联传感器的应变灵敏度进行测试，干涉光谱如图 10 所示，随着应变的增加，干涉光谱均发生红移，级联传感器的包络波长漂移量远高于单个

PMI 波长漂移量，应变灵敏度得到了显著提高。单个 PMI 与级联传感器的应变灵敏度如图 11 所示，测得单个 PMI 的应变灵敏度分别为 13.04 pm/με 和 12.90 pm/με，级联传感器的应变灵敏度为 154.04 pm/με，约是单个 PMI 的 11.81 倍，与理论值 11.34 基本一致。
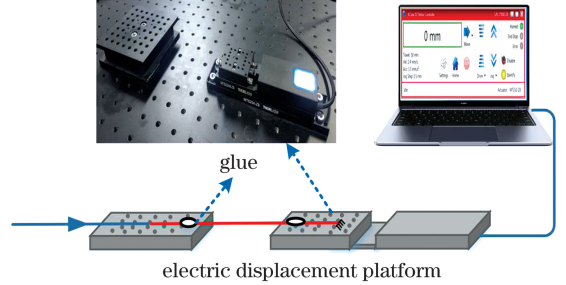

图 9　电位移平台示意图

Fig. 9　Schematic of electric displacement platform
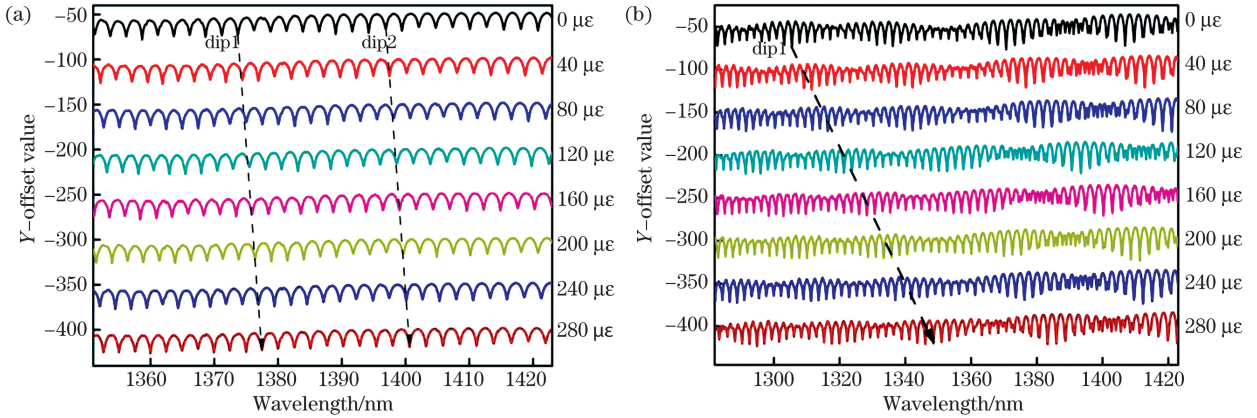
图 10　传感器在不同应变下的干涉光谱。(a)单个 PMI；(b)级联传感器

Fig. 10　Interference spectra of the sensor under different strains. (a) Single PMI; (b) cascaded sensor
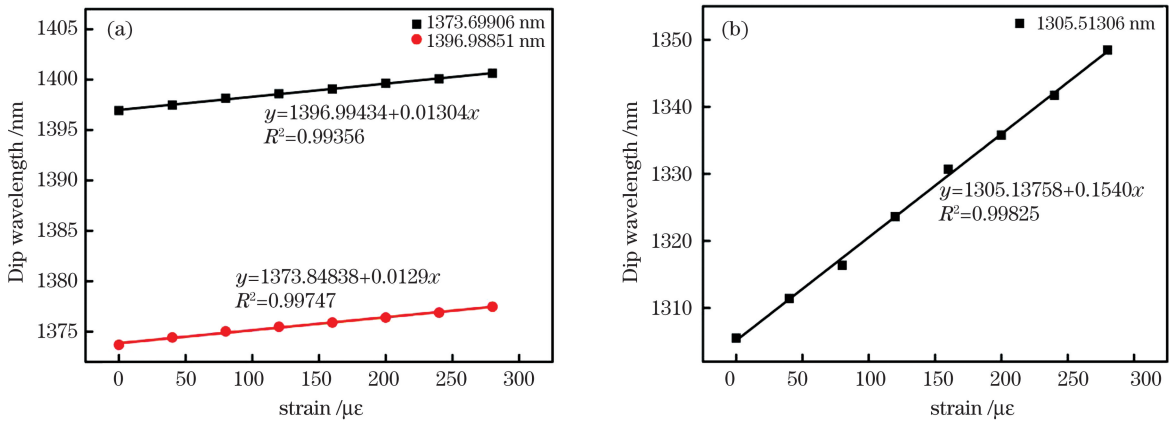

图 11　波长漂移与应变的关系。(a)单个 PMI；(b)级联传感器

Fig. 11　Relationship between wavelength shift and strain. (a) Single PMI; (b) cascaded sensor

为了验证 FSI 的应变相对不敏感性，利用光学黏合剂将 FSI 固定于微位移平台上，测得单个 FSI 干涉光谱的应变响应，如图 12(a)所示，随着应变量

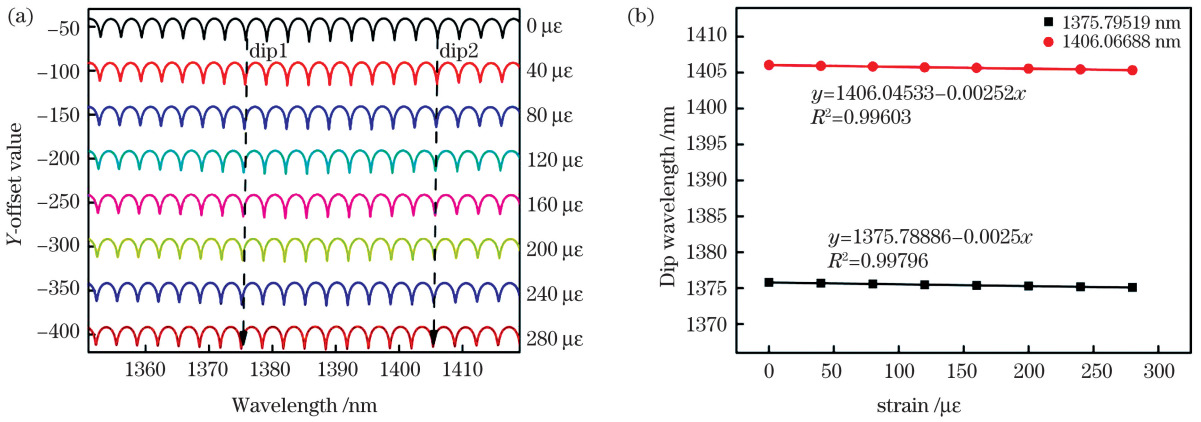的增加，干涉光谱发生蓝移。单个 FSI 的应变灵敏度如图 12(b)所示，测得单个 FSI 的应变灵敏度分别为 2.52pm/με 和 2.50pm/με，约为 PMI 应变灵

图 12　FSI 应变响应。(a)干涉光谱；(b)波长漂移与应变的关系

Fig. 12　Strain response of FSI. (a) Interference spectra; (b) relationship between wavelength shift and strain

敏度的 1/5。因此相对于 PMI，FSI 光谱具有应变不敏感性，用 ECPMF 制备的 FSI 更适合作为参考干涉仪。

4.3　实验结果分析

由以上实验结果可知：级联传感器的温度和应变灵敏度分别为 15.56 nm/℃ 和 154.04 pm/με，与单个 PMI 相比，提高了 11.12 和 11.81 倍；级联传感器的仿真放大因子为 11.34，实验结果和仿真结果基本吻合，误差主要来自于读取光谱时的读数误差。对比图 3(b)和图 5(b)可知，实验所得级联传感器的干涉谱包络的消光比明显低于仿真结果，这是由于在仿真过程中，假设光纤起偏器输出端与一段 PMF 快轴/慢轴熔接角为 45°。实际上，熔接机熔接两个 PMF 时对角有 ±3° 偏差，使得两个偏振模的光强不相等，从而引起条纹可见度降低，但并不影响实验结果。

5　结　　论

提出了一种将 ECPMF 引入 Sagnac 环内作为参考干涉仪的光纤温度和应变传感器。该传感器由参考干涉仪 FSI 和传感干涉仪 PMI 组成，合理设计 PMF 和 ECPMF 的长度，使 FSI 和 PMI 的 FSR 相近但不相等，从而形成游标效应。实验结果表明，该级联传感器的温度和应变灵敏度分别为 15.56 nm/℃ 和 154.04 pm/με，与单个 PMI 相比，温度和应变灵敏度分别提高了 11.12 和 11.81 倍，与仿真结果基本相吻合，证明该方案具有有效性和可靠性。所设计的级联传感器具有灵敏度高、稳定性好、成本低、制作简单等优点，在航空航天和工业生产等领域中具有广阔的应用前景。

参　考　文　献

[1] Chen Y F, Wan H D, Chen Q, et al. High sensitivity optical fiber temperature sensor based on rare-earth-doped double-fiber peanut [J]. Chinese Journal of Lasers, 2020, 47(1): 0110001.
陈彧芳, 万洪丹, 陈乾, 等. 基于稀土光纤双花生结的高灵敏度光纤温度传感器[J]. 中国激光, 2020, 47(1): 0110001.

[2] Wu C, Liu Z Y, Zhang A, et al. In-line open-cavity Fabry-Pérot interferometer formed by C-shaped fiber for temperature-insensitive refractive index sensing [J]. Optics Express, 2014, 22(18): 21757-21766.

[3] Xu J S, He J, Huang W, et al. Suppression of parasitic interference in a fiber-tip Fabry-Perot interferometer for high-pressure measurements[J]. Optics Express, 2018, 26(22): 28178-28186.

[4] Zhang Z L, Gao L, Sun Y Y, et al. Strain transfer law of distributed optical fiber sensor [J]. Chinese Journal of Lasers, 2019, 46(4): 0410001.
章征林, 高磊, 孙阳阳, 等. 分布式光纤传感器应变传递规律研究[J]. 中国激光, 2019, 46(4): 0410001.

[5] Xia X P, Zhang Y M, Lou X P, et al. Half-size metal-packaged fiber Bragg grating for simultaneous measurement of strain and temperature[J]. Optical Engineering, 2019, 58(11): 116104.

[6] Liu Y G, Wang Y X, Yang D Q, et al. Hollow-core fiber-based all-fiber FPI sensor for simultaneous measurement of air pressure and temperature[J]. IEEE Sensors Journal, 2019, 19(23): 11236-11241.

[7] Liu Y, Wang D N. Fiber in-line Fabry-Perot interferometer with offset splicing for strain measurement with enhanced sensitivity [J]. IEEE Photonics Journal, 2018, 10(1): 1-8.

[8] Dong L G, Gang T T, Bian C, et al. A high sensitivity optical fiber strain sensor based on hollow core tapering [J]. Optical Fiber Technology, 2020, 56: 102179.

[9] Sun X Y, Du H F, Dong X R, et al. Simultaneous

curvature and temperature sensing based on a novel Mach-Zehnder interferometer[J]. Photonic Sensors, 2020, 10(2): 171-180.

[10] Shao L P, Hu J H, Lu H L, et al. High-sensitivity temperature sensor based on polarization maintaining fiber Sagnac loop[J]. Photonic Sensors, 2019, 9(1): 25-32.

[11] Lei X Q, Dong X P. High-sensitivity Fabry-Perot interferometer high-temperature fiber sensor based on vernier effect[J]. IEEE Sensors Journal, 2020, 20(10): 5292-5297.

[12] Liao H, Lu P, Fu X, et al. Sensitivity amplification of fiber-optic in-line Mach-Zehnder interferometer sensors with modified vernier-effect[J]. Optics Express, 2017, 25(22): 26898-26909.

[13] Shao L Y, Luo Y, Zhang Z Y, et al. Sensitivity-enhanced temperature sensor with cascaded fiber optic Sagnac interferometers based on vernier-effect[J]. Optics Communications, 2015, 336: 73-76.

[14] Wang X Z, Wang Q. A high-birefringence microfiber Sagnac-interferometer biosensor based on thevernier effect[J]. Sensors, 2018, 18(12): 4114.

[15] Wu B Q, Zhao C L, Xu B, et al. Optical fiber hydrogen sensor with single Sagnac interferometer loop based onvernier effect[J]. Sensors and Actuators B: Chemical, 2018, 255: 3011-3016.

[16] Hao J Q, Han B C. Ultrasensitive refractive index sensor based on optical fiber couplers assisted with vernier effect[J]. Acta Optica Sinica, 2020, 40(2): 0206002.

郝晋青, 韩丙辰. 基于游标效应的高灵敏度光纤耦合器折射率传感器[J]. 光学学报, 2020, 40(2): 0206002.

[17] Wang Z R, Huang L, Liu C, et al. Sensitivity-enhanced fiber temperature sensor based onvernier effect and dual in-line Mach-Zehnder interferometers [J]. IEEE Sensors Journal, 2019, 19(18): 7983-7987.

[18] Yang Y Q, Wang Y G, Zhao Y X, et al. Ultrasensitive temperature sensor based on fiber-optic Fabry-Pérot interferometer with vernier effect[J]. Journal of Russian Laser Research, 2019, 40(3): 243-248.

[19] Su H Y, Zhang Y D, Zhao Y P, et al. Parallel double-FPIs temperature sensor based on suspended-core microstructured optical fiber[J]. IEEE Photonics Technology Letters, 2019, 31(24): 1905-1908.

[20] Liu L, Ning T G, Zheng J J, et al. High-sensitivity strain sensor implemented by hybrid cascaded interferometers and the vernier-effect[J]. Optics & Laser Technology, 2019, 119: 105591.

[21] Liu S, Lu P, Chen E C, et al. Vernier effect of fiber interferometer based on cascaded PANDA polarization maintaining fiber [J]. Chinese Optics Letters, 2019, 17(8): 080601.

[22] Zhong C, Shen C Y, You Y, et al. A polarization-maintaining fiber loop mirror based sensor for liquid refractive index absolute measurement[J]. Sensors and Actuators B: Chemical, 2012, 168: 360-364.

[23] Gomes A D, Becker M, Dellith J, et al. Multimode Fabry-Perot interferometer probe based on vernier effect for enhanced temperature sensing[J]. Sensors, 2019, 19(3): 453.

High-Sensitivity Fiber Optic Temperature and Strain Sensors Based on the Vernier Effect

Fang Shasha[1], Wu Xuqiang[1,2*], Zhang Gang[1], Shi Jinhui[1],
Zuo Cheng[2], Zhang Wujun[2], Gui Lei[2], Yu Benli[1,2]

[1]*Anhui Laboratory of Information Materials and Intelligent Sensing, Anhui University, Hefei, Anhui 230601, China;*
[2]*Key Laboratory of Opto-Electronic Information Acquisition and Manipulation, Ministry of Education,*
Anhui University, Hefei, Anhui 230601, China

Abstract

Objective Optical fiber sensors have been extensively used to measure the external physical properties, such as temperature, refractive index, pressure, and strain, because of their characteristics such as simple structure, compact size, low weight, electromagnetic immunity, and high sensitivity. Generally, the fiber optic temperature and strain sensors are manufactured using fiber Bragg gratings (FBG) and optical fiber interferometers. However, the existing optical fiber sensors cannot meet the requirements in some scenarios that require high measurement sensitivity. Therefore, in this study, we propose using the optical vernier effect to enhance the performances of the optical fiber sensors. Normally, the optical vernier effect is generated by cascading two interferometers, among which one is set as the sensing interferometer and the other is set as the reference interferometer. The current interferometers based on the optical vernier effect generally include two cascading interferometers exhibiting almost

identical responses to external disturbance, decreasing the sensitivity of the system. A complex isolation structure is usually applied to the reference interferometer to increase the response difference of the two interferometers with respect to the external disturbance, increasing the complexity of the sensors. Therefore, it is considerably important to design a reference interferometer not sensitive to the changes in external environment and achieve high-sensitivity and high-accuracy sensing of temperature and strain.

Methods   In this study, a reference interferometer based on the fiber Sagnac interferometer (FSI) is constructed by introducing an elliptical core polarization-maintaining fiber (ECPMF), which exhibits insensitivity to temperature, strain, bending, and torsion. The cascaded sensor is constructed by cascading a reference interferometer and a sensing interferometer based on polarization-mode interferometers (PMI). The optical vernier effect is obtained by controlling the free spectral range (FSR) of the two interferometers to be close but not equal. Thus, high-sensitivity and high-accuracy temperature and strain sensing is realized. The pigtail of the 3-dB coupler of the reference FSI is cut as short as possible to minimize its response to environmental disturbance. The length, major-axis radius, minor-axis radius, and cladding diameter of ECPMF (IVG PME-1300-125) are 10 m, 3 μm, 1 μm, and 125 μm, respectively. The PMI is considered to be the sensing interferometer, which is obtained by splicing a polarizer and a polarization-maintaining fiber (PMF) with the fast/slow axis at of an angle of 45°; the other end of the PMF is gold-coated. The length, core, and cladding diameters of the PMF (YOFC PM1017-A) are 0.94 m, 6.5 μm, and 125 μm, respectively. Furthermore, theoretical analysis, numerical simulation, and experimental verification have been successively conducted based on the above design.

Results and Discussions   The output spectra of single FSI, single PMI, and cascaded sensors are analyzed theoretically and simulated to verify that the vernier effect can improve the system sensitivity. Results show that the FSR of PMI and FSI are 2.87 and 3.15 nm, respectively. When the birefringence parameter of the PMF is increased from 3.5×10^{-4} to 3.51×10^{-4}, the interference spectrum of single PMI exhibits a 1.12-nm red shift, whereas that of the cascaded sensor exhibits a 12.7-nm red shift. The magnification factor is 11.34. When no strain is applied to the fiber at room temperature, the FSR of PMI, FSI, and cascaded sensors are 2.83, 3.1, and 35 nm, respectively. Based on theoretical analysis, the birefringence parameter and beat length of ECPMF are 6×10^{-5} and 25.8 mm at 1550 nm, respectively, which are consistent with the product specifications. The magnification factor with respect to the vernier effect obtained via theoretical calculation is 11.48, which is consistent with the simulation results. FSI and FMI are placed on a heating plate with a precision of 0.01 ℃ to investigate the temperature sensing characteristics of FMI and the relative temperature insensitivity of FSI. In the experiment, the temperature measurement ranges from 30 ℃ to 37 ℃ with a step of 1 ℃; each temperature state is maintained for 20 min. The temperature sensitivities of dip 1 and 2 are 1.40 and 1.38 nm/℃ for a single PMI, respectively, whereas those of dip 1 and 2 are 168.38 and 157.44 pm/℃ for a single FSI, resulting in a temperature sensitivity that is approximately 1/8 of the single PMI temperature sensitivity. Thus, FSI is insensitive to temperature. After being amplified by the vernier effect, the temperature sensitivity of the cascaded sensors becomes 15.56 nm/℃, which is 11.12 times greater than that of a single PMI and is consistent with the theoretical value of 11.34. FSI and PMI are fixed using an optical adhesive (NORLAND 81) on a microdisplacement platform (Thorlabs, KMTS25E/M) with an accuracy of 1 μm to investigate the strain sensing characteristics of PMI and the relative strain insensitivity of FSI, and the distance between the two platforms is 40 cm. Controlled by software, one of the microdisplacement platforms move outward; further, a displacement step of 16 μm and a corresponding PMI strain step of 40 $\mu\varepsilon$ are realized, and the strain measurement range is from 0 to 280 $\mu\varepsilon$. The strain sensitivities of dip 1 and 2 are 13.04 and 12.90 pm/$\mu\varepsilon$ for a single PMI, whereas those of dip 1 and 2 are 2.52 and 2.50 pm/$\mu\varepsilon$ for a single FSI, resulting in a strain sensitivity that is approximately 1/5 of the single PMI strain sensitivity. Thus, FSI is insensitive to strain. After being amplified by the vernier effect, the strain sensitivity of the cascaded sensors becomes 15.56 nm/℃, which is 11.81 times greater than that of a single PMI and is consistent with the theoretical value of 11.34. The deviation in values can be attributed to the manual reading of the spectrum.

Conclusions   In this study, a highly sensitive optical fiber temperature and strain sensor is proposed by introducing ECPMF into the Sagnac ring as a reference interferometer. The sensor includes a reference interferometer FSI and a sensing interferometer PMI, and the lengths of PMF and ECPMF are reasonably designed to make the FSR of FSI and PMI close but not equal, resulting in a vernier effect. The experimental results show that the temperature and strain sensitivity of the cascaded sensor become 15.56 nm/℃ and 154.04 pm/$\mu\varepsilon$, respectively, which are 11.12 and 11.81 times greater than that associated with a single PMI, respectively, and consistent with the simulation results.

Thus, the effectiveness and reliability of the proposed scheme are verified based on the experimental results. The obtained sensor exhibits high sensitivity, a simple structure, good stability, and a good application prospect in various fields such as aerospace and industrial production.